Preprint of: Development. 2022 Sep 15;149(18):dev201184. doi: 10.1242/dev.201184. Epub 2022 Sep 23.

Pivotal role of WUSCHEL-RELATED HOMEOBOX 9/STIMPY in ovule pattern formation and female germline development in *Arabidopsis thaliana*.

Rosanna Petrella[1], Flavio Gabrieli[1], Alex Cavalleri[1], Kay Schneitz[2], Lucia Colombo[1] and Mara Cucinotta[1].

1 Dipartimento di Bioscienze, Università degli Studi di Milano, Via Celoria 26, 20133 Milan, Italy.

2 Plant Developmental Biology, School of Life Sciences, Technical University of Munich, Freising, Germany

*Corresponding author: Mara Cucinotta

Email: mara.cucinotta@unimi.it

Abstract

In spermatophytes the sporophytic (diploid) and the gametophytic (haploid) generations co-exist in ovules, and the coordination of their developmental programs is of pivotal importance for plant reproduction. To achieve efficient fertilization, the haploid female gametophyte and the diploid ovule structures must coordinate their development to form a functional and correctly shaped ovule. *WUSCHEL-RELATED HOMEOBOX (WOX)* genes encode for a family of transcription factors, sharing important roles in a wide range of processes throughout plant development. Here we show that WOX9/STIP is required for the correct patterning and curvature of the ovule. The knockout mutant *stip-2* is characterized by a radialized ovule phenotype due to severe defects in outer integument development. In addition, alteration of *WOX9/STIP* expression affects the correct differentiation and progression of the female germline. Finally, our results reveal that WOX9/STIP is required to tightly regulate the key ovule factors *INNER NO OUTER (INO)*, *PHABULOSA (PHB)* and *WUSCHEL (WUS)* and they define a novel genetic interplay in the regulatory networks determining ovule development.

Introduction

Ovules, which develop into seeds upon fertilization, are fundamental for sexual reproduction. Ovules emerge from the placenta, a meristematic tissue inside the pistil, which represent the female reproductive structure of flowers. Within the Arabidopsis pistil, ovules arise as regularly spaced finger-like protuberances; three different regions are distinguishable along the proximal-distal axis: the nucellus, the chalaza and the funiculus. The nucellus is the most distal region, harboring the female germline precursor, while the funiculus is the most proximal structure which forms a stalk that connects the ovule to the placenta. The chalaza is the central structure, giving rise to the outer integument (OI) and the inner integument (II), which envelop the nucellus, protecting the female gametophyte (Robinson-Beers et al., 1992; Schneitz et al., 1995; Vijayan et al., 2021). In Arabidopsis, an important role of the OI is the establishment of the curvature (anatropy) of the ovule (Endress, 2011). The OI is initiated on the posterior side of the primordium and its asymmetric growth results in a bilateral symmetrical structure of the ovule. The two integuments leave open a minute pore, the micropyle, through which the pollen tube enter the megagametophyte (or embryo sac) during double fertilization. Upon fertilization, integuments will differentiate into the seed coat, sharing a pivotal role in communication between the maternal tissues and the developing embryo (Beeckman et al., 2000; Robert et al., 2018; Hater et al., 2020).

Synchronously with integument development, the female germline precursor, the megaspore mother cell (MMC), undergoes meiosis, forming four haploid megaspores; the three most distal ones degenerate, while the surviving haploid functional megaspore (FM) develops into the seven-celled embryo sac. Interestingly, development of the embryo sac also depends on the integuments, as mutants defective in the asymmetric growth of OI have been reported to show defects in female germline progression as well (Bencivenga et al., 2011; Chevalier et al., 2011; Wang et al., 2016).

In *Arabidopsis thaliana*, the activities of several transcription factors ensure proper formation of integuments and correct embryo sac development (Colombo et al., 2008; Erbasol Serbes et al., 2019; Gasser and Skinner, 2019). Key players of OI formation are *INNER NO OUTER (INO)*, *KANADI 1 (KAN1)* and *KANADI 2 (KAN2)* (Villanueva et al., 1999; McAbee et al., 2006). In leaves, *KAN1* and *KAN2* determine abaxial identity and their activity is antagonized in the adaxial domain by class III HD-ZIP genes, such as *PHABULOSA (PHB)* (Kuhlemeier and Timmermans, 2016). In ovules, *INO* is expressed in the abaxial cell layer of the OI and its activity is necessary for the promotion of cell division in the early OI and in the adjacent chalaza (Balasubramanian and Schneitz, 2000; Vijayan et al., 2021; Villanueva et al., 1999). INO activity is tightly regulated by the transcriptional repressor *SUPERMAN (SUP)*, which prevents overgrowth of the OI (Balasubramanian and Schneitz, 2002; Hiratsu et al., 2002; Meister et al., 2002).

In *Arabidopsis thaliana,* the *WUSCHEL-RELATED HOMEOBOX (WOX)* family comprises 15 members which fulfill specialized functions in key developmental processes such as: embryonic patterning, stem cell maintenance and organ formation (van der Graaff et al., 2009; Wu et al., 2019).

Beside its role in maintaining the stem cell population in the shoot apical meristem, *WUSCHEL* (*WUS*) controls the formation of the chalaza and integument formation in the ovule (Groß-Hardt et al., 2002; Sieber et al., 2004); as matter of fact, lack of *WUS* expression determines ovules that develop without integuments (Groß-Hardt et al., 2002). WOX transcription factors share a DNA-binding homeodomain (HD) (Gehring et al., 1994; Haecker et al., 2004), while other coding regions of the *WOX* genes are highly divergent in sequence (Wu et al., 2019).

Among them, *WUSCHEL-RELATED HOMEOBOX 9/STIMPY* (*WOX9/STIP*), henceforth named *STIP*, in contrast with the other WOX transcription factors, does not carry the typical WUS domain required for both transcriptional repression and activation (Ikeda et al., 2009), but harbors two copies of a relaxed form of the EAR repressive motif (van der Graaff et al., 2009). It has been demonstrated that, in the shoot apical meristem (SAM), *STIP* controls the balance between stem cell maintenance and differentiation, most likely by regulation of *WUS* expression (Wu et al., 2005). In addition, *STIP* acts redundantly with its paralog *WOX8* to define the apical-basal axis in the embryo (Breuninger et al., 2008; Haecker et al., 2004).

Although *STIP* has been reported to be expressed in reproductive structures (Wu et al., 2005), its role in plant fertility has not been investigated yet. Here, we conducted an extensive analysis to dissect the role of *STIP* during ovule development, highlighting a pivotal role for this factor in controlling integument development and female germline progression.

Results

STIP is expressed in developing ovules

Previously, it has been shown that *STIP* is expressed in developing embryos, floral meristems and in emerging floral organs including pistils (Wu et al., 2005). By *in situ* hybridization, we confirmed that in the ovary, *STIP* is expressed in the outermost layer of the placenta (Figure 1A-E) and in the septum (Figure 1D), as previously described (Wu et al., 2005). Furthermore, we detected *STIP* transcript in the funiculus at different ovule developmental stages (Figure 1A-E). To assess whether STIP protein accumulation pattern reflects transcript localization we analysed the expression of *pSTIP:STIP-GFP* reporter (Haecker et al., 2004; Wu et al., 2007). Consistently with the *STIP* transcript, STIP-GFP fusion protein was localized in the epidermal layer of the funiculus in all the different stages analysed (Figure 1F-J). Interestingly, we observed that in ovule primordia at stage 1-II and 2-I, STIP-GFP localization was not restricted to the funiculus but it was also detected in the chalaza and in the epidermal layer of the nucellus (L1), suggesting a possible movement of the STIP-GFP protein (Figure 1F-G). Furthermore, analysis of *GFP* transcript expression in *pSTIP:STIP-GFP* plants by *in situ* hybridization, showed the same expression pattern observed for *STIP* (Figure 1A,B and Supplementary Figure S1), hence excluding that the discrepancy between *STIP* and STIP-GFP pattern was due to lack of regulatory regions in *pSTIP:STIP-GFP.*

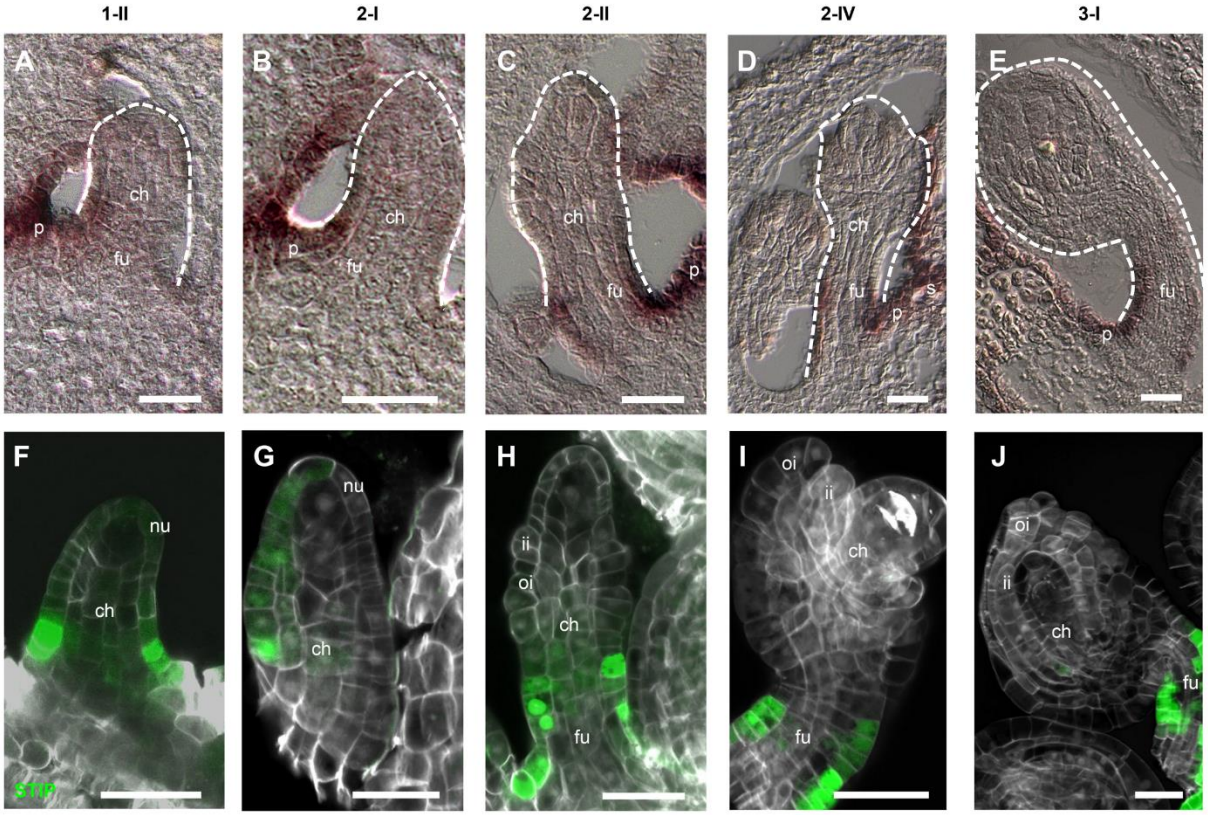

Figure 1. *STIP* expression pattern and protein localization

(A-E) *In situ* hybridization on tissue sections of wild-type ovules using a *STIP* antisense probe. (F-J) Analysis of *pSTIP:STIP-GFP* (Haecker et al., 2004; Wu et al., 2007) expression in the ovule. Abbreviations: p, placenta; fu, funiculus; ch, chalaza; s, septum; nu, nucellus; oi, outer integument; ii, inner integument;. Scale bars, 20 µm.

Ovule development is severely affected in *stip* loss-of-function mutant

To further dissect the role of *STIP* in ovule development we analysed a *STIP* loss-of-function mutant, named *stip-2*, presenting pleiotropic defects throughout plant development (Wu et al., 2005). In particular, *stip-2* plants are impaired in maintaining the vegetative shoot apical meristem (i.e., SAM), resulting in premature seedling lethality, defects that can be overcome by stimulating the cell cycle through the addition of sucrose to the growth medium (Wu et al., 2005). Thus, we could analyse reproductive tissues in this genetic background. Siliques of *stip-2* plants were shorter and ticker compared to the wild-type background, suggesting defects in plant fertility (Figure 2A). We therefore compared seed set in siliques of *stip-2* and wild-type. We could distinguish three phenotypes: aborted ovules (observed as small and yellowish stalks), aborted seeds (whitish and wrinkled structures), and viable seeds (visible as green and turgid structures) (Figure 2A). In *stip-2*, most of the siliques did not contain any viable seeds; in particular, *stip-2* siliques were characterized by around 80% of ovule abortion and 17% of seed abortion (Figure 2B), and thus *stip-2* plants exhibited almost complete sterility.

To further characterize the role of STIP in ovule development, we performed detailed morphological analyses on ovules of the *stip-2* mutant. In wild-type ovules, integuments arise from the chalaza and grow around the nucellus to wrap and protect the female gametophyte (Figure 2C-F), as schematically illustrated in Figure 2G. Analysis of *stip-2* ovules revealed severe defects in OI development (Figure 2H-K). First, the OI initiated later compared to the wild-type (Figure 2C and H,I). In addition, the OI failed to grow properly, forming an amorphous extrusion attached to the chalaza (Figure 2I-K). Such alteration is most likely determined by random divisions of the OI cells, that fail to define the adaxial-abaxial symmetry, a distinctive trait of anatropous ovules (Figure 2K,L). The arrest of OI growth observed in *stip-2* ovules resulted in a radial rather than a bilateral symmetry. In summary, the data suggest that *STIP* is required for proper outer integument development.

Next, we considered whether the loss of *STIP* function could affect female germline establishment and progression. In wild-type, the MMC starts to differentiate at stage 2-I (Figure 2C) and completes its differentiation at stage 2-II (Figure 2D). No evident phenotypes were observed in *stip-2* ovules at these stages, as the MMC appeared to be correctly specified and enlarged within the nucellus (Figure 2H,I).

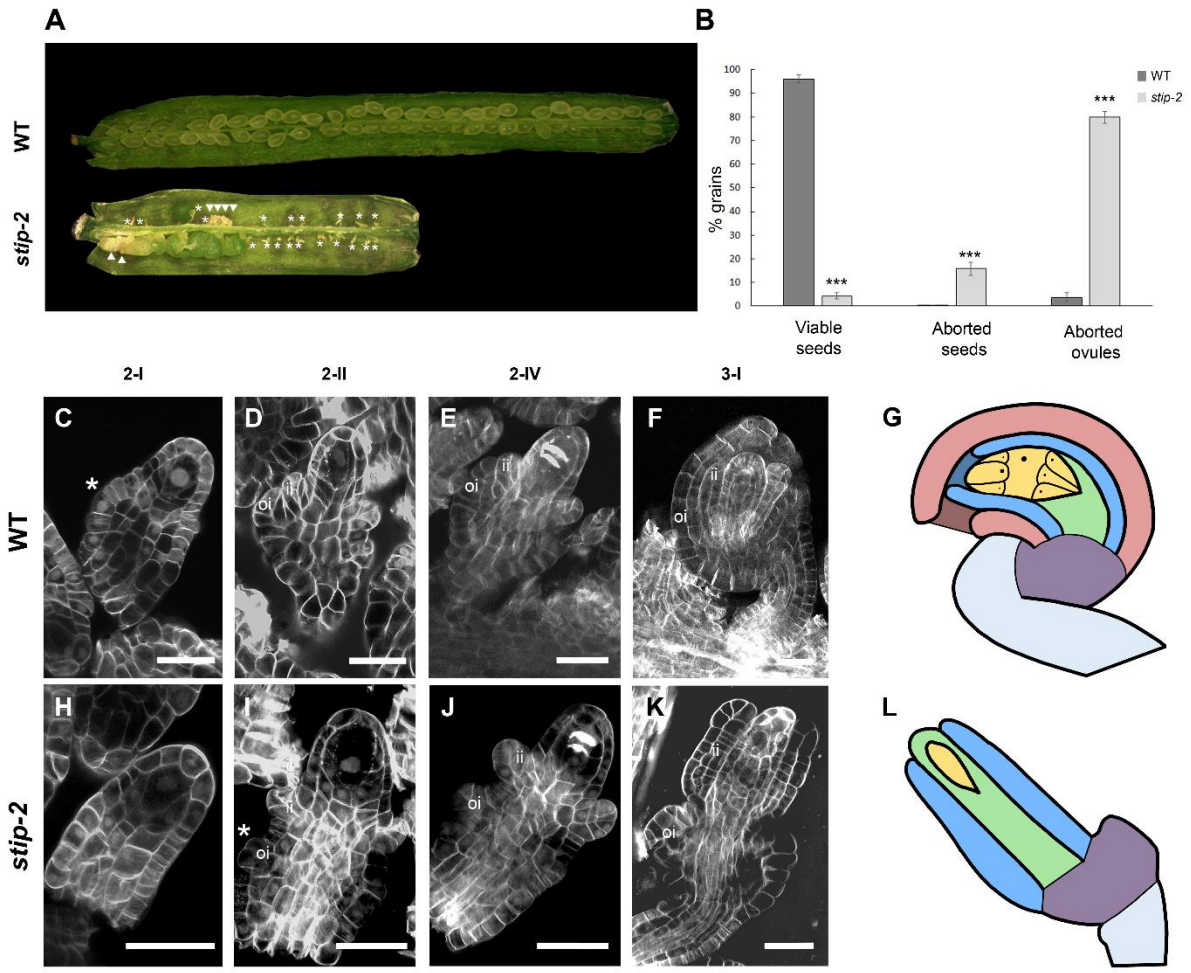

Figure 2. Analysis of *stip-2* reproductive tissues defects.

(A) Seed set of wild-type and *stip-2* siliques. Asterisks indicate aborted ovules and white triangles mark aborted seeds. (B) Frequency of viable seeds, aborted seeds and aborted ovules in wild-type (n=17) and *stip*-2 (n=12) siliques. Data are presented as mean ± standard error (S.E). Asterisks indicate P<0,0001 in Student's t-test, comparing *stip-2* with wild type. (C-F and H-K) SCRI Renaissance 2200 staining in wild-type (C-F) and *stip-2* (H-K) ovules. Abbreviations: oi, outer integument; ii, inner integument. Asterisks indicates site of emergence of ovule integuments. Illustration of wild-type (G) and *stip-2* (L) mature ovules. Pink, outer integument; blue, inner integument; green, nucellus; yellow, female gametophyte; purple, chalaza; light blue, funiculus.

Meiosis process was analysed by looking at callose deposition at the meiotic division plates (Figure 2E and J). We observed apparently normal callose deposition in *stip-2* ovules, suggesting that meiosis occurred normally.

Characterization of subsequent stages, however, revealed that *stip-2* showed defects in megagametogenesis. In particular, analyses of wild-type (n=219) and *stip-2* (n=241) cleared ovules, revealed that in around 94% of *stip-2* ovules, the female gametophyte development was arrested at the FG1 stage (Figure 3A-C). In fact, we could never observe more than one nucleus in the developing female gametophyte (Figure 3A,B). We then investigated the expression of *pLC2::3xnlsYFP*, a marker of the functional megaspore and the two nuclei generated by the first mitotic division (Tucker et al., 2012) (Figure 3D,E). We found that *stip-2* ovules at stage FG1 exhibited normal expression of pLC2::3xnlsYFP (Fig. 3F). By contrast, ovules at later developmental stages showed a faint single signal, most likely localized to the blocked and degenerating functional megaspore (Figure 3G). Our results indicate that the functional megaspore is correctly specified in *stip-2* but that female gametophyte development does not progress, suggesting that *STIP* expression in sporophytic tissue is required for female gametophytic development.

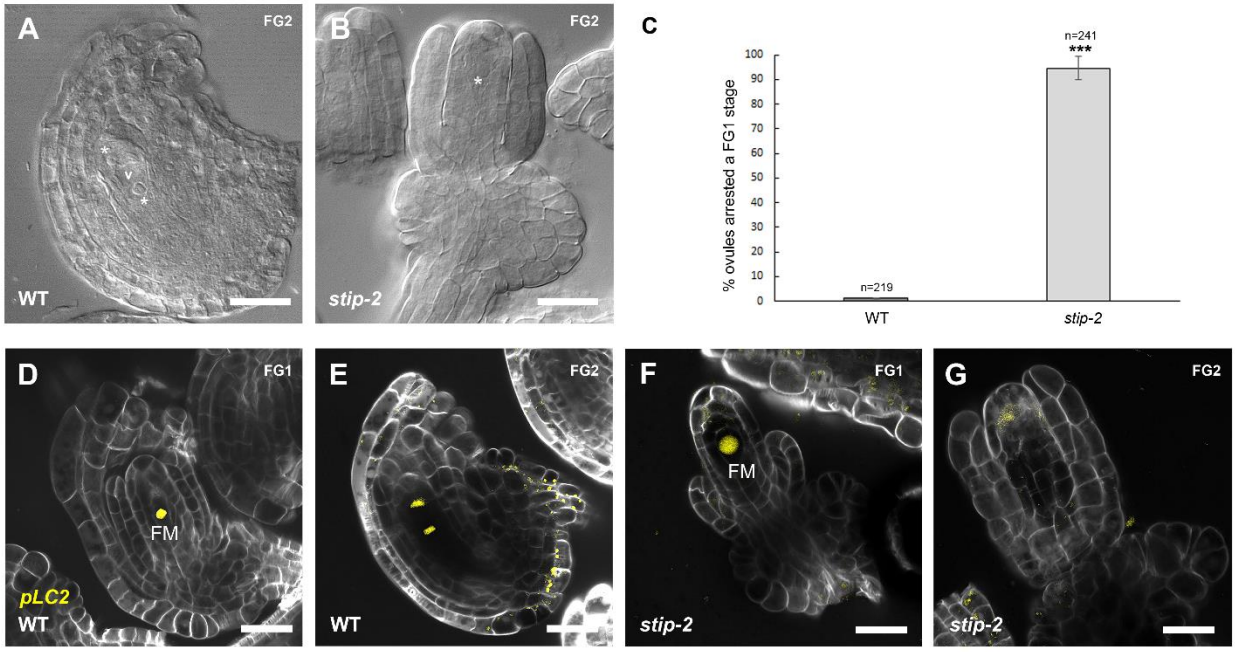

Figure 3. Analysis of megagametogenesis progression and functional megaspore differentiation in *stip-2*.

(A-B) Cleared ovules of wild-type (A) and *stip-2* (B) at FG2 stage. Asterisks indicate FG nuclei; (C) Frequency of ovules arrested at FG1 stage in wild-type (n=219) and *stip-2* (n=241). Data are presented as mean ± S.E. Asterisks indicates P<0,001 in Student's t-test, comparing *stip-2* mutant with wild-type. (D-G) Localization of the *pLC2:3xnlsYFP* reporter (Tucker et al., 2012) in wild-type (D-E) and *stip-2* (F-G). FG1, female gametophyte stage 1; FG2, female gametophyte stage 2. Abbreviations: v, vacuole; FM, functional megaspore. Scale bars, 20 µm.

STIP is required for the expression of *INO*

The analysis described above suggests a role for STIP in the formation of the OI. Several factors have been characterized for their role in OI development, among them, the YABBY transcription factor INO (Villanueva et al., 1999). Mutations in *INO* result in OI arrest (Baker et al., 1997; Schneitz et al., 1997; Vijayan et al., 2021; Figure 4D), a phenotype also observed in *stip-2* ovules (Figure 2K). Even though OI development was severely affected in *ino-5* ovules, morphological analyses revealed no defects in the MMC specification and meiosis progression (Figure 4A-C). By contrast, next stages of female germline development were affected, as we could never detect any progression of the female gametophyte after megasporogenesis (Figure 4D).

As previously showed, *INO* transcript and INO-GFP fusion protein accumulate in the abaxial side of the ovule primordium (Meister et al., 2002; Sieber et al., 2004; Villanueva et al., 1999), at the position where OI will form (Figure 4E,J). In later stages, either *INO* transcript and INO protein are confined to the abaxial layer of OI (Figure 4F-H and L). The expression pattern of *INO* partially overlaps with

STIP protein in the ovule primordium at stage 2-I, preceding OI initiation (Figures 4E,J and Figure 1G). To determine whether *STIP* is required for *INO* expression we investigated *INO* transcript accumulation in *stip-2* by *in situ* hybridization. Ovules of *stip-2* showed no expression of *INO* at different developmental stages (Figure 4M-O). The qRT-PCR confirmed a severe downregulation of *INO* in *stip-2* inflorescences (-4.20 ± 0.01 fold; Figure 4S). Collectively, these results indicate that *STIP* promotes *INO* expression in ovules.

In order to investigate if STIP could directly regulate *INO* expression we analysed *INO* locus for the presence of putative WOX homeodomain consensus sites, by interrogating Plant Pan 3.0 online tool (Chow et al., 2019). Even though we identified four regions with binding sites for WOX transcription factors (Figure 4T; Supplementary Figure 3), we could not detect any enrichment when testing STIP binding by ChIP-PCR assay, thus suggesting an indirect regulation of *INO* by STIP (Figure 4T).

To determine whether STIP activity was not only necessary but also sufficient to drive *INO* expression we analyzed a *stip* mutant carrying a dominant mutation, named *stip-D* (Wu et al., 2005). The mutant was obtained in an activation-tagging screen and it is characterized by the presence of a 35S CAMV enhancer in the 3'UTR region (Wu et al., 2005) (Supplementary Figure 1). By *in situ* hybridization, we determined that *STIP* was ectopically expressed in the chalaza of *stip-D* ovules (Supplementary Figure 1). Upregulation of *STIP* expression was confirmed by qRT-PCR using RNA obtained from inflorescences, showing a significant increase of *STIP* expression (32.7 ± 1.1 fold) compared to the wild-type (Supplementary Figure 1).

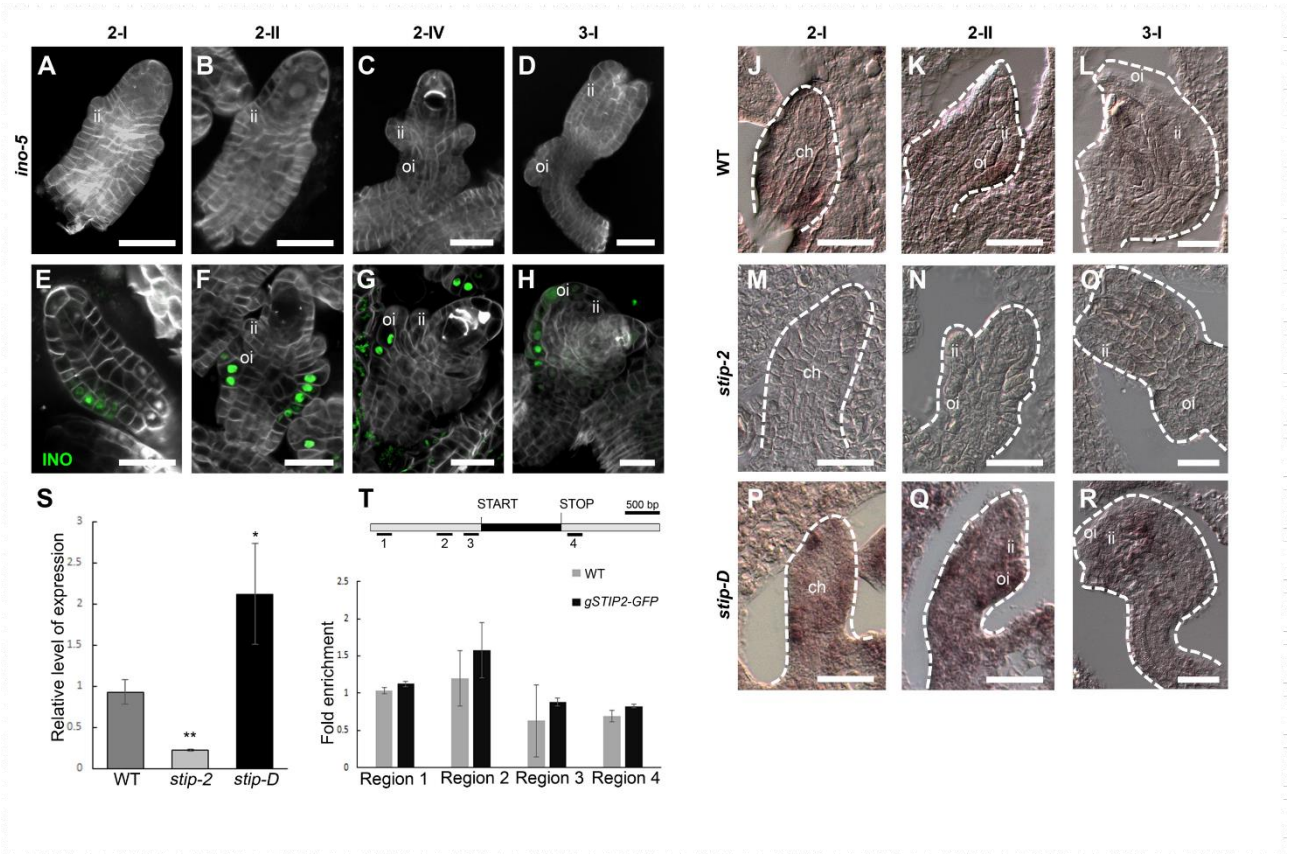

Figure 4. *INO* expression is affected in *STIP* mutant backgrounds.

(A-D) SCRI Renaissance 2200 staining of *ino-5* ovules. (E-H) Analysis of *pINO:INO-GFP* expression in the ovule. (J-R) Detection of *INO* expression by *in situ* hybridization on tissue sections of wild-type (J-L), *stip-2* (M-O) and *stip-D* (P-R) ovules using a *INO* antisense probe. (S) Expression analysis of *INO* by qRT-PCR in wild-type, *stip-2* and *stip-D* inflorescences. Expression of *INO* was normalized to that of *UBIQUITIN10* and the expression level in wild-type was set to 1. Asterisks indicate *P<0,05 and **P<0,01 in Student's t-test, respectively. (T) Schematic diagram of *INO* locus. Black box, exons and introns; grey boxes, promoter and 3' untranslated region; black lines, regions tested by ChIP. Fold change enrichment of ChIP-PCR using chromatin extracted from *pSTIP:STIP-GFP* and wild-type inflorescences (as a negative control), testing the putative binding regions for STIP on *INO* locus. Error bars represent the propagated error value. ChIP-PCR results of one representative experiment are shown. No regions resulted enriched in three independent biological replicates. Abbreviations: ch, chalaza; ii, inner integument; oi, outer integument. Scale bars, 20 µm.

Analysis of *INO* expression in *stip-D* ovules by *in situ* hybridization revealed that *INO* was no longer confined to few cells of the chalaza but it was ectopically expressed in the ovule (compare Figure 4J, K with Figure 4P,Q). In addition, *INO* transcript levels decrease after megasporogenesis in wild-type (Figure 4L); in contrast, we could observe *INO* expression in *stip-D* ovules at stage 3-I (Figure 4R). Likewise, qRT-PCR confirmed an upregulation of *INO* expression in *stip-D* background (+1.51 ± 0.06 fold; Figure 4S). These results indicated that *STIP* is not only required but also sufficient to induce *INO* expression in the ovule.

To assess the effect of *STIP* overexpression on ovule development, we analysed ovule morphology in *stip-D*. *STIP* ectopic expression caused a reduced fertility, with 37% and 23% of ovule and seed abortion, respectively (Figure 5A,B). In comparison to wild-type ovules, *stip-D* exhibited shorter integuments that failed to enclose the developing female gametophyte (Figure 5C,D). In addition, we observed a different shape and position of the MMC within the L2 domain of the nucellus (compare Figure 2C,D with Figure 5C). To determine whether this defect reflected altered MMC development we introduced the MMC-specific *pKNU:3xnlsYFP* reporter (Tucker et al., 2012) into *stip-D* (Figure 5F,G). Although we could not detect any decrease in the number of ovules showing fluorescence, in around 67% of *stip-D* ovules (n=86) the MMC was confined at the tip of the L2 layer of the nucellus (Figure 5E-G and K). Intriguingly, this phenotype was never observed in the wild-type, neither in *stip-2* (Figure 5K). Despite the different localization of the MMC, megasporogenesis apparently progressed as in wild-type. Furthermore, *stip-D* ovules exhibited a mild phenotype in female germline progression, as 37% of *stip-D* ovules were blocked at the FG1 stage (Figure 5H-J). Collectively, these data indicate that mis-regulation of *STIP* result in severe defects in ovule development.

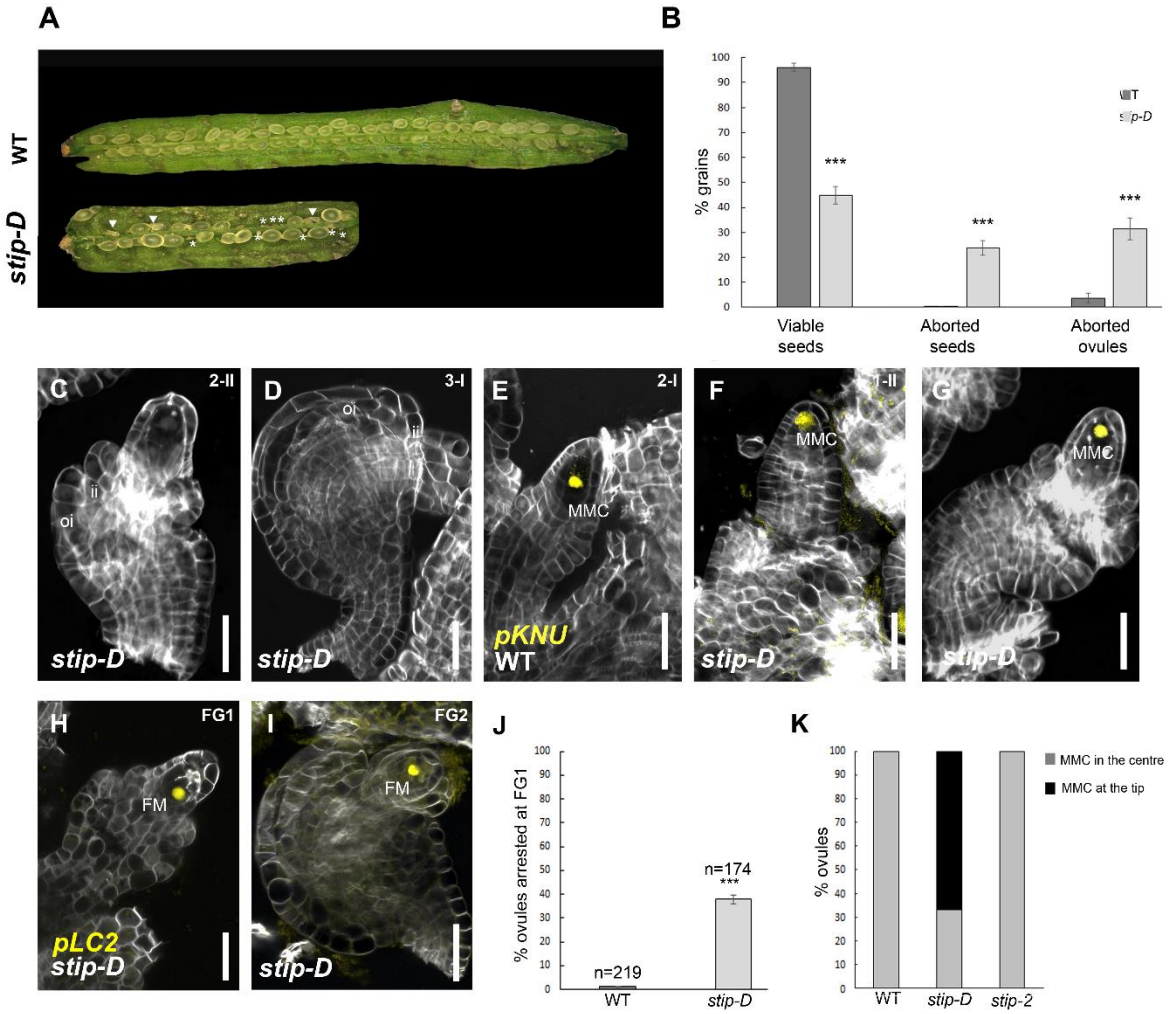

Figure 5. Analysis of *stip-D* reproductive tissues defects.

(A) Seed set in wild-type and *stip-D*. Asterisks indicate aborted ovules and white triangles mark aborted seeds. (B) Frequency of viable seeds, aborted seeds and aborted ovules in wild-type (n=17) and *stip*-D (n=12) siliques. Asterisks indicates P<0,0001 in Student's t-test, comparing *stip-D* with wild-type. Data are presented as mean ± S.E. (C-D) SCRI Renaissance 2200 staining of *stip-D* ovules. (E-G) *pKNU:3xnlsYFP* expression in wild type (E) and *stip-D* at two different stages: 2-I (F) and 2-II (G). (H-I) Expression of *pLC2:3xnlsYFP* in *stip-D*. (J) Frequency of ovules arrested at FG1 stage in wild-type (n=219) and *stip-D* (n=174). Data are presented as mean ± S.E. Asterisks indicate P<0,001 in Student's t-test, comparing *stip-D* mutants with wild-type. (K) Frequency of MMCs placed in the centre and at the tip of the of L2 layer of the nucellus in wild-type (n=51), *stip-D* (n=86), and *stip-2* (n=54) ovules. FG1, female gametophyte stage 1; FG2, female gametophyte stage 2. Abbreviations: oi, outer integument; ii, inner integument; MMC, megaspore mother cell; FM, functional megaspore; Scale bars, 20 µm.

***STIP* directly represses *PHB* expression in the ovule**

It has been previously suggested that *INO* expression is confined to the epidermal layer of OI primordia by class III HD-ZIP factors antagonistic activity (Arnault et al., 2018; Sieber et al., 2004). Among class III HD-ZIP factors, *PHABULOSA (PHB)* has been identified as a putative target of STIP by a high throughput yeast one hybrid screening (Taylor-Teeples et al., 2015). Thus, to determine whether *INO* downregulation in *stip-2* was caused by a deregulation of *PHB* we analysed *PHB* expression in wild-type and *stip-2* ovules by *in situ* hybridization. As previously reported, *PHB* is specifically expressed in the adaxial side of the early ovule primordium (Sieber et al., 2004; Figure 6A). During the later stages of ovule development, *PHB* expression is confined to the chalaza where the inner integument initiates (Figure 6B,C). We could not detect any differences in *PHB* expression in the early ovule primordium of *stip-2* (Figure 6D). However, at a later stage we observed ectopic *PHB* expression in the nucellus (Figure 6E,F), suggesting a role for STIP in repressing *PHB* expression in this domain. In order to test whether STIP could directly bind *PHB* regulatory region *in vivo* we performed a ChIP-PCR experiment, using *pSTIP:STIP-GFP* inflorescences. We identified six putative regions associated to WOX homeodomain transcription factors binding on *PHB* genomic locus (Figure 6G and Supplementary Figure 3) using Plant Pan 3.0 (Chow et al., 2019). Interestingly, we could detect enrichment in two out the six regions tested, suggesting that STIP directly represses *PHB* expression (Figure 6G).

Class III HD-ZIP factors, such as PHB, have been characterized as regulators of the HOMEOBOX gene *WUS* in the shoot apical meristem and in the ovule (Lee and Clark, 2015; Yamada et al., 2015). Considering *WUS* pivotal function in ovule pattern definition (Groß-Hardt et al., 2002; Sieber et al., 2004) and *PHB* ectopic expression in *stip-2*, we analysed *WUS* expression in both *stip* mutants by *in situ* hybridization. As previously reported, *WUS* is strongly expressed in the tip of the early ovule primordium (Figure 7A). We could observe a drastic reduction of *WUS* expression in *stip-2* ovules (Figure 7A,B) whereas *WUS* seems to be overexpressed in *stip-D* (Figure 7A, C). In order to confirm

the downregulation of *WUS* in *stip-2* ovules we analysed *pWUS:eGFP-WUS* (Yamada et al., 2011) reporter line in wild-type (Figure 7D) and *stip-2* (Figure 7E) backgrounds. WUS-GFP is localized in the nucellar cells surrounding the MMC (Figure 7D). As expected, we observed a strong decrease of WUS-GFP signal in *stip-2* nucellar cells, compared to the wild-type (Figure 7D-F), showing the importance of STIP for the regulation of *WUS* in the nucellus.

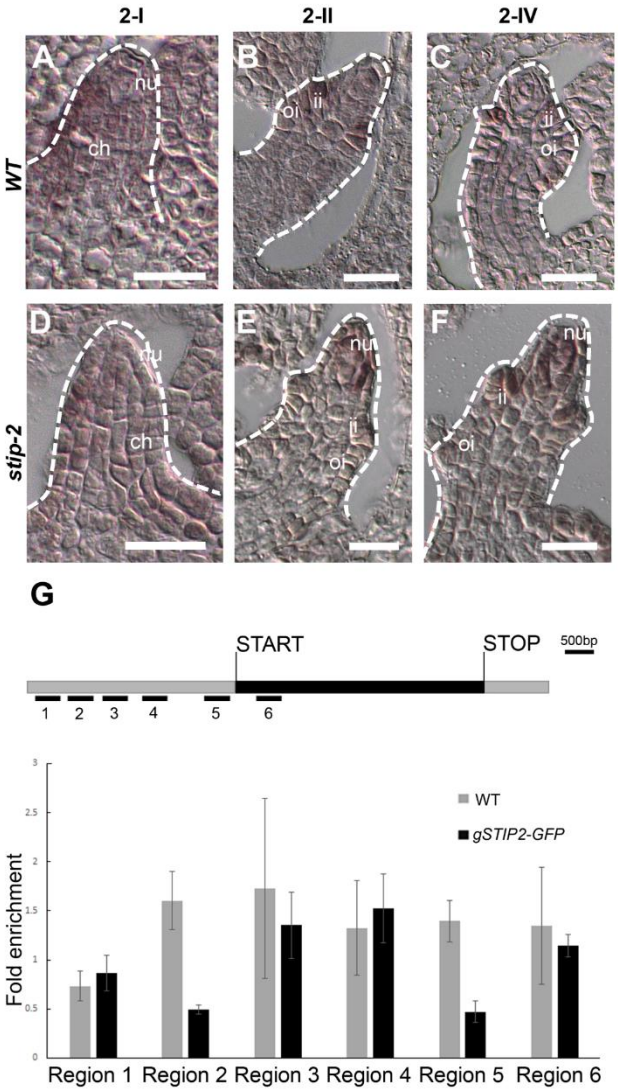

Figure 6. STIP directly regulates *PHB* expression in the ovule.

(A-F) *In situ* hybridization on ovule tissue sections using *PHB* antisense probe. Expression of *PHB* in wild-type (A-C) and *stip-2* (D-F). (G) Schematic diagram of *PHB* locus. Black box, exons and introns; grey boxes, promoter and 3' untranslated region; black lines, regions tested by ChIP. Fold change enrichment of ChIP-PCR using chromatin extracted from *pSTIP:STIP-GFP* and wild-type inflorescences (as a negative control), testing the putative binding regions for STIP on *PHB* locus. Error bars represent the propagated error value. Results from one representative experiment are shown and two out of six regions (Region 2 and Region 5) resulted enriched in two independent biological replicates. Abbreviations: ch, chalaza, nu, nucellus; oi, outer integument; ii, inner integument. Scale bars, 20 µm.

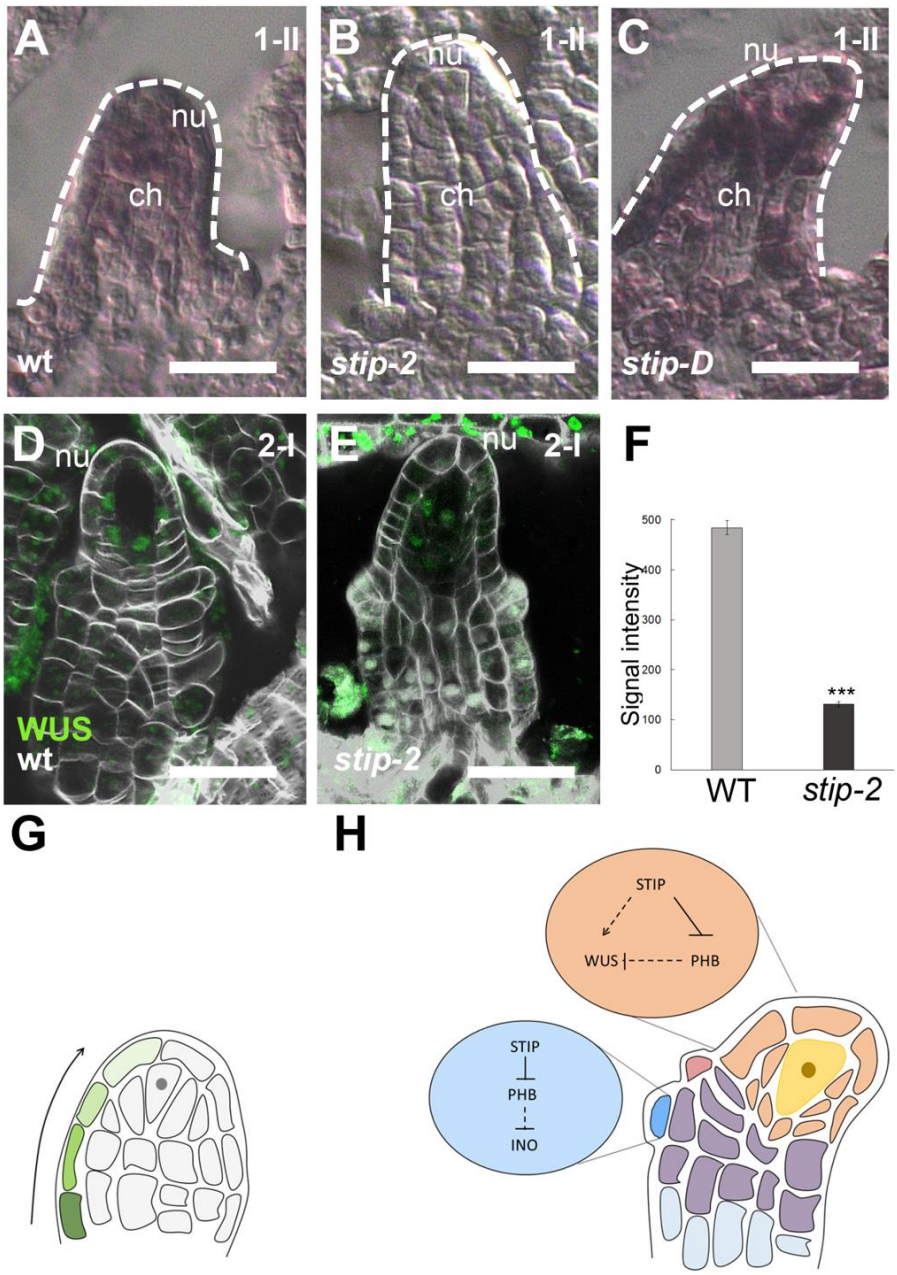

313

314 **Figure 7. WUS expression in the nucellus relies on STIP activity** (A-C) Expression of *WUS* in wild type
315 (A), *stip-2* (B) and *stip-D* (C). (D,E) Expression of *pWUS:eGFP-WUS* in wild-type (D) and *stip-2* (E). (F) Signal
316 intensity measurement of WUS-GFP in nucellar cells of wild-type and *stip-2* ovules. Data are presented as
317 mean ± S.E. Asterisks indicate P<0,001 in Student's t-test, comparing s*tip-2* mutant with wild-type.
318 Abbreviations: ch, chalaza, nu, nucellus. Scale bars, 20 µm. (G) Schematic model proposing movement of
319 STIP protein along the epidermal layer of the ovule. Gradient of green shades and arrow represent the
320 movement of the protein, dark green represents domain of *STIP* transcript accumulation. (H) Model of the
321 proposed STIP-dependent genetic network. In the abaxial layer of the OI, STIP positively regulates *INO*
322 expression by directly repressing *PHB.* In the L1 layer of the nucellus, STIP activates *WUS* expression most
323 likely by directly repressing *PHB* or by activating *WUS*. Color code: orange, nucellus; yellow, megaspore
324 mother cell (MMC); violet, chalaza; light blue, funiculus; pink, inner integument primordium; blue, outer
325 integument primordium. Drawings adapted from Petrella et al., 2021.

Discussion

WUSCHEL-RELATED HOMEOBOX gene family has been previously shown to regulate plant organogenesis, controlling cell proliferation and differentiation (Tvorogova et al., 2021). Here we identified *STIP* as a pivotal gene for proper ovule integument development and female germline progression. *STIP* loss-of-function (*stip-2)* and gain-of-function (*stip-D)* mutants are characterized by severe defects in OI formation and female germline arrest. Intriguingly, we detected a different pattern of expression between the *STIP* transcript and the STIP-GFP fusion protein. In fact, *STIP* transcript was confined to the placenta and the funiculus throughout ovule development. In contrast, we observed localization of the STIP-GFP protein in the epidermal layer of the anterior side of the ovule, up to the tip of the nucellus at stage I-II and 2-I. The observed discrepancy between *STIP* transcript accumulation and protein pattern is consistent with the previous suggestion that STIP acts as a non-cell autonomous transcription factor in the embryo (Haecker et al., 2004; Wu et al., 2007). The movement of WOX factors (e.g., WOX2 and WOX5) was indeed reported to be necessary for their activity in embryo and root development (Daum et al., 2014; Haecker et al., 2004). In addition, stem cell maintenance in the shoot apical meristem required WUS movement (Yadav and Reddy, 2012). Despite that, Gross-Hardt and colleagues (2002) observed that WUS protein does not move in the ovule primordium. Based on our data, we suggest that during early ovule development STIP moves from the funiculus to the epidermal layer of the chalaza and the nucellus, impacting on early ovule patterning (Figure 7G). In this scenario, STIP regulates the expression of the YABBY gene *INO*, which is specifically expressed on the abaxial side of ovule primordia at the site of OI initiation. We indeed showed that STIP is required for *INO* expression, since *stip-2* is characterized by low or no *INO* expression in the ovule. Furthermore, *stip-2* and *ino-5* share a similar phenotype, showing severe defects in OI formation.

Meister et al., (2005) previously reported that INO could promote its own expression in a positive regulative loop to maintain ovule polarity throughout ovule development. Thus, STIP might trigger *INO* expression to determine OI identity, successively maintained by the INO autoregulative loop. On the other hand, *stip-D* is characterized by ectopic expression of *INO* as its expression is no longer confined to the abaxial side of the ovule. *INO* upregulation could affect its downstream pathways and most likely trigger not yet defined mechanisms, thus resulting in the aberrant cell division in both outer and inner integument, observed in the *stip-D* mutant. Interestingly, *superman (sup)* mutants show disorganised divisions of ovule integuments. *SUP* has been reported to act as a negative regulator of *INO*, restricting its expression to the abaxial layer of the ovule primordium (Balasubramanian and Schneitz, 2002; Meister et al., 2002), confirming that spatial confinement of *INO* is fundamental for ovule patterning and OI identity.

It has been shown that class III HD-ZIP factors cooperatively act to determine ovule integument patterning (Gasser and Skinner, 2019). In particular, PHB has been reported to non-autonomously

repress *INO* expression in the adaxial layer of OI (Gasser and Skinner, 2019). Interestingly, we showed that *PHB* expression is directly regulated by STIP in the ovule. Loss of *STIP* function resulted in ectopic expression of *PHB*. Thus, STIP might act as a positive regulator of *INO* expression through the repression of *PHB* in the abaxial side of the emerging OI. However, *in situ* hybridization showed ectopic *PHB* expression in the nucellus but no alteration of *PHB* expression in the chalaza of *stip-2* ovules. It has been reported that *miR166D* post-transcriptionally represses *PHB* to confine its expression in the integument primordia (Hashimoto et al., 2018). Therefore, the transcriptional deregulation of *PHB* by *STIP* could be balanced by MIR166D repression activity. As matter of fact, we observed ectopic expression of *PHB* in the nucellus, where *MIR166* is not expressed (Hashimoto et al., 2018). Collectively, these results support a role for *STIP* in repressing *PHB* activity to achieve a correct ovule development.

We also reported a role for *STIP* in female germline development, as the analyzed *stip* mutants showed defects in this process. We did not observe any defects in the establishment of the female germline in the loss-of-function mutant *stip-2.* By contrast, we noticed that ectopic expression of *STIP* caused a mis-localization of *pKNU:3xnlsYFP* expression, suggesting that *STIP* overexpression might affect MMC morphology. *STIP* was reported to be a positive regulator of *WUS* expression in the SAM (Wu et al., 2005). In the ovule primordium, *WUS* is transiently expressed mainly in the epidermal nucellus before and after MMC specification (Groß-Hardt et al., 2002; Sieber et al., 2004; Vijayan et al., 2021). Here, *WUS* activity is required for the formation of the female germline and its expression needs to be excluded from the MMC for meiosis to occur (Lieber et al., 2011; Zhao et al., 2017). Our results confirmed a positive regulation of *WUS* expression by *STIP* also in the ovule as its expression is noticeably reduced in *stip-2* ovules. In addition, we could detect a clear signal in the epidermal layer of the chalaza and the nucellus of *stip-D* ovules. It has been already reported that several factors expressed in the L1 layer of the nucellus could non-autonomously regulate MMC specification and progression (Mendes et al., 2020; Olmedo-Monfil et al., 2010; Petrella et al., 2021; Su et al., 2020). Thus, altering *WUS* expression levels in *stip-D* ovules could result in the observed altered position of the MMC, that can still undergo meiosis.

PHB acts redundantly with other class III HD-ZIP genes to confine *WUS* expression to the nucellus (Yamada et al., 2015). Our results support a role of *PHB* in repressing *WUS* expression, since *stip-2* ovules are characterized by ectopic expression of *PHB* which could result in the observed reduced levels of *WUS* expression in the nucellus. We propose a model in which *STIP* regulates proper OI development by activating *INO* expression via *PHB* repression (Figure 7H). Furthermore, we put forward the notion of a *STIP-WUS-PHB* genetic cascade contributing to the determination of female germline development.

Since we could never detect *STIP* expression in the L2 layer of the nucellus or in the female germline cells we propose that STIP functions non-cell-autonomously in female gametophyte development. A communication between sporophytic and gametophytic tissues has long been proposed, since

mutations in other transcription factor genes, such as *BELL1 (BEL1)* and *AINTEGUMENTA (ANT)*, affect the formation of integuments and the gametophyte (Bencivenga et al., 2012; Grossniklaus and Schneitz, 1998; Skinner et al., 2004). *STIP* functional characterization corroborated the hypothesis of a crosstalk between generations, required for female gametophytic development, suggesting that a tight regulation of *STIP* expression in the sporophytic tissue is required to ensure female germline progression.

STIP expression is positively regulated by cytokinins in the shoot apical meristem (Skylar et al., 2010). In this context, STIP has been shown to activate the expression of several cytokinin response genes, thus mediating cytokinin signalling and the maintenance of meristematic fate. In light of this, we could speculate that STIP might non-autonomously orchestrate gametogenesis via the regulation of cytokinin signalling as perturbation of cytokinin pathways resulted in an early arrest of embryo sac development at the FG1 stage (Cheng et al., 2013). Hence, STIP could be a key modulator of cytokinin signalling in the ovule. All in all, our results unravelled a new role for STIP in ovule integument formation and female germline progression and contribute to the ongoing dissection of the molecular network regulating ovule development in *Arabidopsis thaliana*.

Materials and Methods

Plant material and growth conditions

Arabidopsis thaliana plants Columbia-0 (Col-0) and Landsberg *erecta* (Ler) ecotype were used for the experiments. The *stip-2* (Wu et al. 2005), *stip-D* (Weigel et al., 2000), *pSTIP::STIP:GFP* (Wu et al., 2007) and *pINO:INO-GFP* (Skinner et al., 2016). *pKNU:nlsYFP* and *pLC2:nlsYFP* (pAt5g40730:nls-vYFP) markers (Tucker et al., 2012) in wild-type background were crossed with *stip-D* and *stip-2* mutants and three homozygous F2 plants were analyzed for expression. *pWUS:eGFP-WUS* (Yamada et al., 2011) in wild-type background were crossed with *stip-2* mutant and three homozygous F2 plants were analyzed for expression. Seeds were sown in soil and then stored at 4°C in dark for two days before moving them to short day (SD) with 8 h of light and 16 h of dark. After a couple of weeks plants were moved in long day (LD), with 16 h of light per day. To recover shoot apical meristem phenotype, *stip-2* mutants had been sown in plates with ½ Murashige & Skoog (MS/2) growth medium supplemented with sucrose to a final concentration of 1.5%. After the “breaking” of dormancy plates were moved to a growth chamber (16 h of light per day, 8 h of dark per day, 23°C, 70% humidity) for 10 days. Then plants were transferred in soil and placed in LD condition.

Seed set analysis and fertilization efficiency

Seed set was analyzed using a stereomicroscope Leica MZ6; 12-14 days after pollination (DAP) siliques were collected from three different plants for wild-type (n=17), *stip-2* (n=12) and *stip-D* (n=12). The three genotypes were analyzed in the same experiment. Fruits were placed onto glass

slides using double-sided adhesive tape and their valves were opened using syringe needles. Structures emerging from the septum were catalogized and counted for each silique collected as viable seeds, aborted seeds, or aborted ovules. Statistical analysis was performed by calculating the average number for each class; standard errors of the mean (SAM) were also calculated.

Optical microscopy

Cleared ovules were analyzed using DIC microscopy (Zeiss Axiophot D1 ×63) to assess the percentage of ovules arrested at FG1 stage. Pictures were acquired with a Zeiss Axiocam MRc5 camera and Axiovision (version 4.1) software.

Confocal microscopy

Confocal laser scanning microscopy of ovules stained with SR2200 was performed on a Nikon Eclipse Ti2 inverted microscope, equipped with a Nikon A1R+ laser scanning device (http://www.nikon.com/). Images were acquired by a CFI Apo Lambda 40XC LWD WI (Numerical Aperture (NA) 1.15). NIS-Elements (Nikon; http://www.nis-elements.com/) was used as a platform to control the microscope. Nondenoised images were analyzed using NIS-Elements and Fiji. SR2200 was excited with a 405 nm laser line and emission detected between 415 and 476 nm, whereas eYFP and eGFP were excited at 488 nm and detected at 498–530 nm. Glasses were prepared using a stereomicroscope; for the observation of ovules, pistils were excised from the flowers and covered by a drop of RS2200 solution (0.1% v/v; kept in the dark).

RNA extraction and gene expression analysis

Quantitative real-time PCR experiments were performed using cDNA obtained from inflorescences. Total RNA was extracted with phenol:chloroform and precipitated using lithium chloride. RNA samples were treated for gDNA contamination and retrotrascribed with iScript™ gDNA Clear cDNA Synthesis Kit (bio-rad Laboratories). Transcripts were detected using a SYBR Green Assay (iQ SYBR Green Supermix; Bio-Rad Laboratories) using *UBIQUITIN10* as a housekeeping gene. Assays were performed in triplicate using a Bio-Rad iCycler iQ Optical System (software v.3.0a). The enrichments were calculated normalizing the amount of mRNA against housekeeping gene fragments. The expression of different genes was analyzed using specific oligonucleotides primers (Table Supplementary Table 1).

In situ hybridization assay

Arabidopsis flowers were collected, fixed, and embedded in paraffin, as described by Galbiati et al., (2013). Plant tissue sections were probed with *WOX9, INO, PHB*, *WUS* and *GFP* antisense probes, described in Wu et al., (2015), Villanueva et al., (1999) and Seiber et al., (2004). Sense probes are

shown in Supplementary Figure 2. Hybridization and immunological detection were executed as described previously by Galbiati et al., (2013).

Chromatin immunoprecipitation assay (ChIP)

To determine putative binding regions for STIP on *INO* and *PHB* loci (Supplementary Figure 3) we interrogated the Plant Pan3.0 online tool (http://plantpan.itps.ncku.edu.tw; Chow et al., 2019). ChIP assays were performed as described by Gregis et al., (2013) using inflorescences (comprises inflorescence meristem and closed buds) from wild-type and *pSTIP:STIP-GFP* using an anti-GFP antibody (Roche, 11814460001), coupled with Dynabeads™ Protein G for Immunoprecipitation (ThermoFisher, 10003D) (4ng of antibody for 30µl of Dynabeads™ Protein G). Real-time PCR assays were performed to determine the enrichment of the fragments. The detection was performed in triplicate using the iQ SYBR Green Supermix (Bio-Rad) and the Bio-Rad iCycler iQ Optical System (software version 3.0a), with the primers listed in Supplementary Table 1. ChIP-qPCR experiments were evaluated according to the fold enrichment method (Gregis et al., 2013). Fold enrichment was calculated using the following formulas: dCT.tg = CT.i-CT.tg and dCT.gapdh = CT.i-CT.gapdh. Ct.tg is target gene mean value, Ct.i is input DNA mean value, and Ct.gapdh is negative control mean value. The propagated error values of these CTs were calculated using dSD.tg = sqrt((SD.i)^2+ (SD.tg^2)/sqrt(*2*) and dSD.gapdh = sqrt((SD.i)^2+ (SD. gapdh^2)/sqrt(*2*). Fold change compared with negative control was calculated by finding the ddCT of the target region as follows: ddCT = dCT.tg− dCT.gapdh and ddSD = sqrt((dSD.tg)^2+ (dSD.gapdh)^2. Transformation to linear fold-change values was performed as follows: FC = 2^(ddCT) and FC.error = ln(2)*ddSD*FC. STIP binding to INO and PHB loci were evaluated in three and two independent replicates, respectively. One representative result was shown for each region tested.

Analysis of WUS-GFP intensity

WUS-GFP intensity measurements in wild-type and *stip-2* backgrounds were performed using Fiji ImageJ software (version 2.1.2). Confocal settings were optimized in the wild-type background and maintained without any changes throughout images acquisition. In order to evaluate the nuclear GFP signal of nucellar cells the GFP channel was used to generate a binary mask by manual thresholding, enlightening all nuclei with WUS-GFP expression. Nuclei belonging to ovules nucella were automatically identified by the particle analyzer tool. GFP signal was then measured in the identified nuclei. The analysis was performed on five wild-type and six *stip-2* ovules at stage 2-I (corresponding to 46 and 61 nucellar cells showing WUS-GFP signal, respectively).

Competing interests

The authors declare no competing or financial interests.

Author contributions

Conceptualization: R.P., L.C., M.C.; Formal analysis and investigation: R.P., F.G., A.C.; M.C., Data Curation: R.P, M.C. Writing – original draft: R.P. Writing – review and editing: R.P., A.C., K.S., L.C., M.C. Funding acquisition: L.C.; Resources: K.S, L.C.

Funding

M.C. was supported by Linea2 - PSR2021, Bioscience Department, University of Milan and by MIUR-PRIN2012. R.P. was supported by MAD Project H2020-MSCA-RISE-2019. K.S. was supported by the German Research Council through grant FOR2581 (TP7).

Acknowledgments

We thank Letizia Cornaro and Tejasvinee Mody for their help. We thank Cecilia Zumajo-Cardona for scientific discussion and thoughtful comments. Part of this work was carried out at NOLIMITS, an advanced imaging facility established by the Università degli Studi di Milano.

References

Arnault, G., Vialette, A. C. M., Andres-Robin, A., Fogliani, B., Gâteblé, G. and Scutt, C. P. (2018). Evidence for the Extensive Conservation of Mechanisms of Ovule Integument Development Since the Most Recent Common Ancestor of Living Angiosperms. *Front. Plant Sci.* **9**,.

Baker, S. C., Robinson-beers, K., Villanueva, J. M., Gaiser, J. C., Gasser, C. S. and Ap, A. (1997). Interactions Among Genes Regulating Ovule Development in Arabidopsis thaliana. *Genetics*. **145**(4):1109-24.

Balasubramanian, S. and Schneitz, K. (2000). NOZZLE regulates proximal-distal pattern formation, cell proliferation and early sporogenesis during ovule development in Arabidopsis thaliana. *Development* **127**, 4227–4238.

Balasubramanian, S. and Schneitz, K. (2002). NOZZLE links proximal-distal and adaxial-abaxial pattern formation during ovule development in Arabidopsis thaliana. *Development* **129**, 4291.

Beeckman, T., De Rycke, R., Viane, R. and Inzé, D. (2000). Histological Study of Seed Coat Development in Arabidopsis thaliana. *J. Plant Res.* **113**, 139–148.

Bencivenga, S., Colombo, L. and Masiero, S. (2011). Cross talk between the sporophyte and the megagametophyte during ovule development. *Sex. Plant Reprod.* **24**, 113–121.

Bencivenga, S., Simonini, S., Benková, E. and Colombo, L. (2012). The transcription factors BEL1 and SPL are required for cytokinin and auxin signaling during ovule development in Arabidopsis. *Plant Cell* **24**, 2886–97.

Breuninger, H., Rikirsch, E., Hermann, M., Ueda, M. and Laux, T. (2008). Differential expression

of WOX genes mediates apical-basal axis formation in the Arabidopsis embryo. *Dev Cell* **14**, 867-76.

Cheng, C.-Y., Mathews, D. E., Eric Schaller, G. and Kieber, J. J. (2013). Cytokinin-dependent specification of the functional megaspore in the Arabidopsis female gametophyte. *Plant J.* **73**, 929–40.

Chevalier, É., Loubert-Hudon, A., Zimmerman, E. L. and Matton, D. P. (2011). Cell–cell communication and signalling pathways within the ovule: from its inception to fertilization. *New Phytol.* **192**, 13–28.

Chow, C.-N., Lee, T.-Y., Hung, Y.-C., Li, G.-Z., Tseng, K.-C., Liu, Y.-H., Kuo, P.-L., Zheng, H.-Q. and Chang, W.-C. (2019). PlantPAN3.0: a new and updated resource for reconstructing transcriptional regulatory networks from ChIP-seq experiments in plants. *Nucleic Acids Res.* **47**, D1155–D1163.

Colombo, L., Battaglia, R. and Kater, M. M. (2008). Arabidopsis ovule development and its evolutionary conservation. *Trends Plant Sci.* **13**, 444–50.

Daum, G., Medzihradszky, A., Suzaki, T. and Lohmann, J. U. (2014). A mechanistic framework for noncell autonomous stem cell induction in Arabidopsis. *Proc. Natl. Acad. Sci.* **111**, 14619–14624.

Endress, P. K. (2011). Angiosperm ovules: diversity, development, evolution. *Ann. Bot.* **107**, 1465–89.

Erbasol Serbes, I., Palovaara, J. and Groß-Hardt, R. (2019). Development and function of the flowering plant female gametophyte. *Curr Top Dev Biol*. **131**:401-434.

Galbiati, F., Sinha Roy, D., Simonini, S., Cucinotta, M., Ceccato, L., Cuesta, C., Simaskova, M., Benková, E., Kamiuchi, Y., Aida, M., et al. (2013). An integrative model of the control of ovule primordia formation. *Plant J.* **76**, 446–55.

Gasser, C. S. and Skinner, D. J. (2019). Development and evolution of the unique ovules of flowering plants. *Curr Top Dev Biol.* **131**:373-399.

Gehring, W. J., Qian, Y. Q., Billeter, M., Furukubo-Tokunaga, K., Schier, A. F., Resendez-Perez, D., Affolter, M., Otting, G. and Wüthrich, K. (1994). Homeodomain-DNA recognition. *Cell* **78**, 211–223.

Gregis, V., Andrés, F., Sessa, A., Guerra, R. F., Simonini, S., Mateos, J. L., Torti, S., Zambelli, F., Prazzoli, G. M., Bjerkan, K. N., et al. (2013). Identification of pathways directly regulated by SHORT VEGETATIVE PHASE during vegetative and reproductive development in Arabidopsis. *Genome Biol.* **14**, R56.

Groß-Hardt, R., Lenhard, M. and Laux, T. (2002). WUSCHEL signaling functions in interregional communication during Arabidopsis ovule development. *Genes Dev.* **16**, 1129–1138.

Grossniklaus, U. and Schneitz, K. (1998). The molecular and genetic basis of ovule and megagametophyte development. *Semin. Cell Dev. Biol.* **9**, 227–238.

584 **Haecker, A., Groß-Hardt, R., Geiges, B., Sarkar, A., Breuninger, H., Herrmann, M. and Laux, T.**
585 (2004). Expression dynamics of WOX genes mark cell fate decisions during early embryonic
586 patterning in Arabidopsis thaliana. *Development* **131**, 657–668.
587 **Hashimoto, K., Miyashima, S., Sato-Nara, K., Yamada, T. and Nakajima, K.** (2018). Functionally
588 Diversified Members of the MIR165/6 Gene Family Regulate Ovule Morphogenesis in
589 Arabidopsis thaliana. *Plant Cell Physiol.* **59**, 1017–1026.
590 **Hater, F., Nakel, T. and Groß-Hardt, R.** (2020). Reproductive Multitasking: The Female
591 Gametophyte. *Annu. Rev. Plant Biol.* **71**, 517–546.
592 **Hiratsu, K., Ohta, M., Matsui, K. and Ohme-Takagi, M.** (2002). The SUPERMAN protein is an
593 active repressor whose carboxy-terminal repression domain is required for the development of
594 normal flowers. *FEBS Lett.* **514**, 351–354.
595 **Ikeda, M., Mitsuda, N. and Ohme-Takagi, M.** (2009). Arabidopsis WUSCHEL Is a Bifunctional
596 Transcription Factor That Acts as a Repressor in Stem Cell Regulation and as an Activator in
597 Floral Patterning. *Plant Cell* **21**, 3493–3505.
598 **Yadav, R.K., Perales, M., Gruel, J., Girke, T., Jönsson, H., Reddy, G.V.** (2011). WUSCHEL
599 protein movement mediates stem cell homeostasis in the Arabidopsis shoot apex. *Genes Dev*.
600 **1**, 2025-30.
601 **Kuhlemeier, C. and Timmermans, M. C. P.** (2016). The Sussex signal: insights into leaf
602 dorsiventrality. *Development* **143**, 3230–3237.
603 **Lee, C. and Clark, S. E.** (2015). A WUSCHEL-Independent Stem Cell Specification Pathway Is
604 Repressed by PHB, PHV and CNA in Arabidopsis. *PLoS One* **10**, e0126006.
605 **Lieber, D., Lora, J., Schrempp, S., Lenhard, M. and Laux, T.** (2011). Arabidopsis WIH1 and WIH2
606 Genes Act in the Transition from Somatic to Reproductive Cell Fate. *Curr. Biol.* **21**, 1009–1017.
607 **McAbee, J. M., Hill, T. A., Skinner, D. J., Izhaki, A., Hauser, B. A., Meister, R. J., Venugopala**
608 **Reddy, G., Meyerowitz, E. M., Bowman, J. L. and Gasser, C. S.** (2006). ABERRANT TESTA
609 SHAPE encodes a KANADI family member, linking polarity determination to separation and
610 growth of Arabidopsis ovule integuments. *Plant J.* **46**, 522–531.
611 **Meister, R. J., Kotow, L. M. and Gasser, C. S.** (2002). SUPERMAN attenuates positive INNER NO
612 OUTER autoregulation to maintain polar development of Arabidopsis ovule outer integuments.
613 *Development* **129**, 4281–4289.
614 **Meister, R. J., Oldenhof, H., Bowman, J. L. and Gasser, C. S.** (2005). Multiple Protein Regions
615 Contribute to Differential Activities of YABBY Proteins inReproductive Development. *Plant*
616 *Physiol.* **137**, 651–662.
617 **Mendes, M. A., Petrella, R., Cucinotta, M., Vignati, E., Gatti, S., Pinto, S. C., Bird, D. C., Gregis,**
618 **V., Dickinson, H., Tucker, M. R., et al.** (2020). The RNA-dependent DNA methylation pathway
619 is required to restrict SPOROCYTELESS/NOZZLE expression to specify a single female germ
620 cell precursor in Arabidopsis. *Development* **147**,.

Olmedo-Monfil, V., Durán-Figueroa, N., Arteaga-Vázquez, M., Demesa-Arévalo, E., Autran, D., Grimanelli, D., Slotkin, R. K., Martienssen, R. A. and Vielle-Calzada, J.-P. (2010). Control of female gamete formation by a small RNA pathway in Arabidopsis. *Nature* **464**, 628–632.

Petrella, R., Cucinotta, M., Mendes, M. A., Underwood, C. J. and Colombo, L. (2021). The emerging role of small RNAs in ovule development, a kind of magic. *Plant Reprod.* **34**, 335–351.

Robert, H. S., Park, C., Gutièrrez, C. L., Wójcikowska, B., Pěnčík, A., Novák, O., Chen, J., Grunewald, W., Dresselhaus, T., Friml, J., et al. (2018). Maternal auxin supply contributes to early embryo patterning in Arabidopsis. *Nat. Plants* **4**, 548–553.

Robinson-Beers, K., Pruitt, R. E. and Gasser, C. S. (1992). Ovule Development in Wild-Type Arabidopsis and Two Female-Sterile Mutants. *Plant Cell* **4**, 1237–1249.

Schneitz, K., Hulskamp, M. and Pruitt, R. E. (1995). Wild-type ovule development in Arabidopsis thaliana: a light microscope study of cleared whole-mount tissue. *Plant J.* **7**, 731–749.

Schneitz, K., Hulskamp, M., Kopczak, S. D. and Pruitt, R. E. (1997). Dissection of sexual organ ontogenesis: a genetic analysis of ovule development in Arabidopsis thaliana. *Development* **124**, 1367–1376.

Sieber, P., Gheyselinck, J., Gross-Hardt, R., Laux, T., Grossniklaus, U. and Schneitz, K. (2004). Pattern formation during early ovule development in Arabidopsis thaliana. *Dev. Biol.* **273**, 321–334.

Skinner, D. J., Hill, T. A. and Gasser, C. S. (2004). Regulation of Ovule Development. *Plant Cell.* **16** *S32-45.*

Skinner, D. J., Brown, R. H., Kuzoff, R. K. and Gasser, C. S. (2016). Conservation of the role of INNER NO OUTER in development of unitegmic ovules of the Solanaceae despite a divergence in protein function. *BMC Plant Biol.* **16**, 143.

Skylar, A., Hong, F., Chory, J., Weigel, D. and Wu, X. (2010). STIMPY mediates cytokinin signaling during shoot meristem establishment in Arabidopsis seedlings. *Development.* **137**, 541–549.

Su, Z., Wang, N., Hou, Z., Li, B., Li, D., Liu, Y., Cai, H., Qin, Y. and Chen, X. (2020). Regulation of female germline specification via small RNA mobility in arabidopsis. *Plant Cell* **32**, 2842–2854.

Taylor-Teeples, M., Lin, L., de Lucas, M., Turco, G., Toal, T. W., Gaudinier, A., Young, N. F., Trabucco, G. M., Veling, M. T., Lamothe, R., et al. (2015). An Arabidopsis gene regulatory network for secondary cell wall synthesis. *Nature* **517**, 571–575.

Tucker, M. R., Okada, T., Hu, Y., Scholefield, A., Taylor, J. M. and Koltunow, A. M. G. (2012). Somatic small RNA pathways promote the mitotic events of megagametogenesis during female reproductive development in Arabidopsis. *Development* **139**, 1399–1404.

Tvorogova, V. E., Krasnoperova, E. Y., Potsenkovskaia, E. A., Kudriashov, A. A., Dodueva, I. E. and Lutova, L. A. (2021). What Does the WOX Say? Review of Regulators, Targets,

Partners. *Mol. Biol.* **55**, 311–337.

van der Graaff, E., Laux, T. and Rensing, S. A. (2009). The WUS homeobox-containing (WOX) protein family. *Genome Biol.* **10**, 248.

Vijayan, A., Tofanelli, R., Strauss, S., Cerrone, L., Wolny, A., Strohmeier, J., Kreshuk, A., Hamprecht, F. A., Smith, R. S. and Schneitz, K. (2021). A digital 3D reference atlas reveals cellular growth patterns shaping the Arabidopsis ovule. *Elife* **10**,.

Villanueva, J. M., Broadhvest, J., Hauser, B. A., Meister, R. J., Schneitz, K. and Gasser, C. S. (1999). INNER NO OUTER regulates abaxial- adaxial patterning in Arabidopsis ovules. *Genes Dev.* **13**, 3160–3169.

Wang, J.-G., Feng, C., Liu, H.-H., Ge, F.-R., Li, S., Li, H.-J. and Zhang, Y. (2016). HAPLESS13-Mediated Trafficking of STRUBBELIG Is Critical for Ovule Development in Arabidopsis. *PLOS Genet.* **12**, e1006269.

Weigel, D., Ahn, J. H., Blázquez, M. A., Borevitz, J. O., Christensen, S. K., Fankhauser, C., Ferrándiz, C., Kardailsky, I., Malancharuvil, E. J., Neff, M. M., et al. (2000). Activation Tagging in Arabidopsis. *Plant Physiol.* **122**, 1003–1014.

Wu, X., Dabi, T. and Weigel, D. (2005). Requirement of homeobox gene STIMPY/WOX9 for Arabidopsis meristem growth and maintenance. *Curr. Biol.* **15**, 436–440.

Wu, X., Chory, J. and Weigel, D. (2007). Combinations of WOX activities regulate tissue proliferation during Arabidopsis embryonic development. *Dev. Biol.* **309**, 306–16.

Wu, C.-C., Li, F.-W. and Kramer, E. M. (2019). Large-scale phylogenomic analysis suggests three ancient superclades of the WUSCHEL-RELATED HOMEOBOX transcription factor family in plants. *PLoS One* **14**, e0223521.

Yadav, R. K. and Reddy, G. V. (2012). WUSCHEL protein movement and stem cell homeostasis. *Plant Signal. Behav.* **7**, 592–594.

Yamada, T., Sasaki, Y., Hashimoto, K., Nakajima, K. and Gasser, C. S. (2015). CORONA , PHABULOSA and PHAVOLUTA collaborate with BELL 1 to confine WUSCHEL expression to the nucellus in Arabidopsis ovules. *Development*. **143**(3):422-6.

Zhao, X., Bramsiepe, J., Van Durme, M., Komaki, S., Prusicki, M. A., Maruyama, D., Forner, J., Medzihradszky, A., Wijnker, E., Harashima, H., et al. (2017). RETINOBLASTOMA RELATED1 mediates germline entry in Arabidopsis. *Science.***356**, eaaf6532.

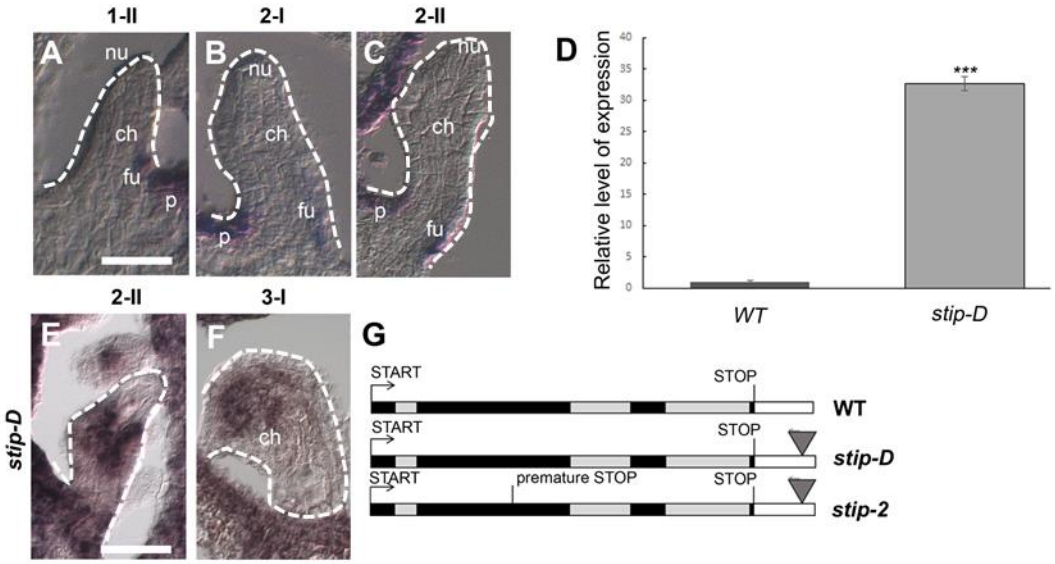

695

696 **Supplementary Figure 1.**

697 (A-C) *In situ* hybridization on ovule tissue sections of *pSTIP:STIP-GFP*, using a *GFP* antisense probe. (D)
698 Expression analysis of *STIP* by qRT-PCR in wild-type and *stip-D* inflorescences. Expression of *STIP* was
699 normalized to that of *UBIQUITIN10* and the expression level in wild-type was set to 1. Asterisks indicate
700 P<0.0001 in Student's t-test. (E-F) *In situ* hybridization on ovule tissue sections of *stip-D*, using a *STIP*
701 antisense probe. (G) Schematic diagram of the *STIP* locus in wild-type, *stip-D*, and *stip-2.* As reported by Wu
702 et al., (2005; 2007) *stip-2* mutation has the same genetic background of *stip-D* (it harbors a T-DNA in the
703 3'UTR), but it presents a mis-match in the coding region, generating a premature stop codon, leading to a
704 knock-out mutation. Black boxes, exons; grey boxes, introns; white box, 3'untranslated region; T-DNA insertion
705 is represented with a grey triangle. Abbreviations: ch, chalaza; nu, nucellus; p, placenta; fu, funiculus. Scale
706 bar, 20 µm.

707

708

709

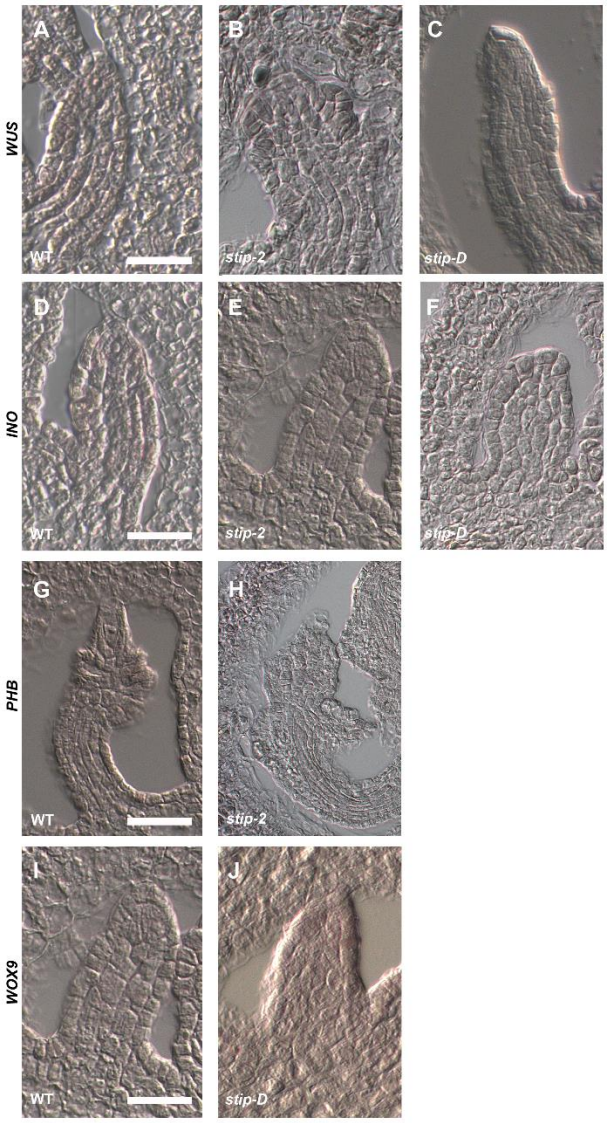

Supplementary figure 2.

(A-J) Sense probe controls for the all the *in situ* hybridization assays performed: *WUS* (A-C), *INO* (D-F), *PHB* (G-H) and *WOX9* (I,J). Scale bars, 20 µm.

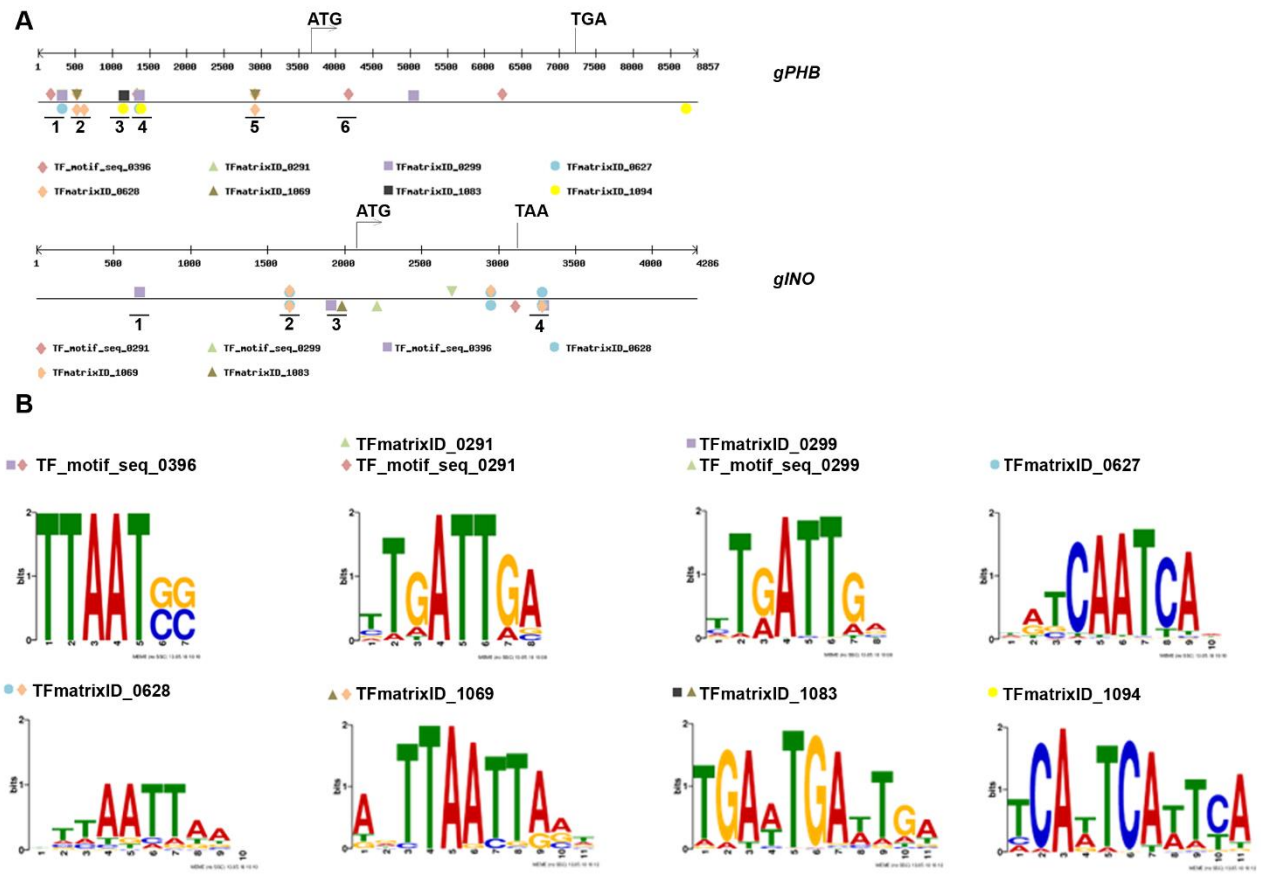

Supplementary Figure 3.

(A) Schematic representation of WOX homeodomain binding site in *PHB* and *INO* loci. The regions tested in STIP-GFP ChIP-PCR assays are marked with black lines and numbered. (B) Consensus logo of binding sequences of WOX homeodomain transcription factors detected on *PHB* and *INO* loci. Analysis was performed using PlantPan 3.0 ((http://plantpan.itps.ncku.edu.tw).

Primer sequence	**Description**
GCTCACCATTGATCGTGTGGGAGATTTGAG	*stip-2*/*stip-D* Fw genotyping
ACCACGTCTTCAAAGCAAGTG	*stip-2/stip-D* Rv genotyping
GAAGCAATCTTTAACTCCGGG	*stip-2* Fw sequencing
AGAGAAACCCTAATTGGGAT	*stip-2* Rv sequencing
GTTTCTCTTCCCGGTCTCCA	*WOX9* Fw for ISH probe
ACAGTAGCGAGAGAATGC	*WOX9* Rv for ISH probe
TAATACGACTCACTATAGGGGTTTCTCTTCCCGGTCTCCA	*WOX9* Fw + T7 for ISH probe
TAATACGACTCACTATAGGGGACAGTAGCGAGAGAATGC	*WOX9* Rv + T7 for ISH probe
TGCCATGTCCAGTGTGGTTT	*INO* Fw for ISH probe
AGGCTTGTGCAATGCCCA	*INO* Rv for ISH probe
TAATACGACTCACTATAGGGTGCCATGTCCAGTGTGGTTT	*INO* Fw + T7 for ISH probe
TAATACGACTCACTATAGGGAGGCTTGTGCAATGCCCA	*INO* Rv + T7 for ISH probe
GAAGAAGAATGTGGTGGCG	*WUS* Fw for ISH probe
GAGAGAGAGAGGAAAGAGC	*WUS* Rv for ISH probe
TAATACGACTCACTATAGGGAAGAAGAATGTGGTGGCG	*WUS* fw + pT7 for ISH probe
TAATACGACTCACTATAGGGAGAGAGAGAGGAAAGAGC	*WUS* Rv + T7 for ISH probe
GGTAGCGATGGTGCAGAGG	*PHB* Fw for ISH probe
CGAACGACCAATTCACGAAC	*PHB* Rv for ISH probe
TAATACGACTCACTATAGGGGGTAGCGATGGTGCAGAGG	*PHB* ISH fw + T7 for ISH probe
TAATACGACTCACTATAGGGCGAACGACCAATTCACGAAC	*PHB* ISH rv + T7 for ISH probe
GTTTCTCTTCCCGGTCTCCA	*INO* Fw RT-qPCR
ACAGTAGCGAGAGAATGC	*INO* Rv RT-qPCR
CCAATTAGGGTTTCTCTCCGG	*WOX9* Fw RT-qPCR
TCCCTCACATTGAACGGTCC	*WOX9* Rv RT-qPCR
CTGTTCACGGAACCCAATTC	*UBI* Fw RT-qPCR
GGAAAAAGGTCTGACCGACA	*UBI* Rv RT-qPCR
CGTTTCGCTTTCCTTAGTGTTAGCT	*ACT7* Fw qPCR
AGCGAACGGATCTAGAGACTCACCTTG	*ACT7* Rv qPCR
ACCAAAGCATTCCACATGAAAGA	*pINO* R1 Fw qPCR
GGAGCTTTGTCATAGAGAGTGTGT	*pINO* R1 Rv qPCR
ACTGCTTACAGCTCATAGAGAC	*pINO* R2 Fw qPCR

TCTTTCATGTGGAATGCTTTGGT	*pINO* R2 Rv qPCR
GACTGTTAAACCAGAAGCCATAACT	*pINO* R3 Fw qPCR
GACCCAACCCCGGAGTGAA	*pINO* R3 Rv qPCR
TTACACTACGGACGGCTCTGA	*pINO* R4 Fw qPCR
CCAGTAAAGGATCGTTAACATGTAC	*pINO* R4 Rv qPCR
CAACTGAAAACGTTTGTAGACTCTAGTC	*pPHB R1 fw qPCR*
CAAGGTGATCGTACCATTATGAAGTTC	*pPHB R1 rv qPCR*
GCACTCATTGTGCATCGCTTATC	*pPHB R2 fw qPCR*
CCACGCTTTTATCTCGTTTCATATGTG	pPHB R3 fw qPCR
CTCCAGCAACCAAACTATTCACTC	pPHB R4 fw qPCR
CGTGTTACCAATTTACCAATCAAAATC	pPHB R4 rv qPCR
GTGAAGGTTTAGTCGCATCCTTC	pPHB R5 fw qPCR
GGCTTTTCTCCTTTATTGTCTTTCCC	pPHB R5 rv qPCR
GTTTCTTCTGGTTATAACTTGTGATGC	pPHB R6 fw qPCR
GTTTCCTTGCTGTTCTTATCTGACAAG	pPHB R6 rv qPCR

732

733 **Supplementary table 1.** List of primers used in this study.